MRI Guided Myocardial Perfusion PET Image Reconstruction

Jing Tang, *Member, IEEE*, Xinhui Wang, Nicolas A. Karakatsanis, *Member, IEEE*, Lijun Lu, and Arman Rahmim, *Senior Member, IEEE*

***Abstract*–Integrated whole-body PET/MRI provides opportunities to fully take advantage of simultaneously acquired anatomical and functional information. The purpose of this study is to incorporate the MR measured anatomical information in myocardial perfusion (MP) PET image reconstruction and to quantitatively evaluate the reconstructed images. Using the 4D XCAT phantom, we simulated cardiac-gated MP PET data with and without a perfusion defect and the corresponding MR images. Noisy PET sinograms were generated with count levels comparable to patient Rb-82 MP PET measurement. MR images were simulated using the SIMRI simulator, with the MR sequence specified to be 3D T1-weighted as used in a clinical PET/MRI protocol. For each cardiac gate, we applied the closed-form maximum *a posteriori* (MAP) PET image reconstruction taking the joint-entropy (JE) between intensity of the PET and MR images as the prior. To quantitatively evaluate the reconstructed images, we used the tradeoff between bias and noise on the left ventricle polar map. The contrast recovery ratio was also calculated to quantify the ability to classify the polar maps with and without the MP defect. On the whole polar map and its segments, the activity values estimated from the JE MAP algorithm showed significantly improved noise versus bias tradeoff compared to those from the conventional maximum likelihood algorithm. The JE MAP algorithm also resulted in improved noise versus contrast recovery for the MP defect. To conclude, we demonstrated quantitatively improved performance of the anato-functional JE MAP reconstruction on MP PET imaging with realistic simulation. The reconstruction technique will have promising potential applications especially in the emerging integrated cardiac PET/MR imaging.**

I. Introduction

THE arrival of integrated whole-body PET/MRI provides new opportunities and challenges to fully take advantage of the simultaneous acquisition of anatomical and functional information [1]. MR image based attenuation correction is critical in quantitative PET image reconstruction and has been broadly studied [2, 3]. Works have also been carried out on motion compensated PET imaging using motion estimated from simultaneously taken MR images [4, 5]. Before the availability of integrated PET/MRI, techniques on using anatomical information to assist PET image reconstruction have been developed [6]. However, very few studies have been performed on cardiac imaging. This is most likely due to the complicating issues of cardiac motion and of the difficulties in registering the PET and MR images, prior to the advent of the simultaneous acquisition capability.

We developed a Bayesian image reconstruction technique incorporating the joint-entropy (JE) of PET and MR image features as the regularization constraint [7]. The technique was applied and evaluated with simulated and patient brain data. In this study, we propose to use MR information for myocardial perfusion (MP) PET image reconstruction. Using realistically simulated cardiac-gated PET data and MR images, our goal is to evaluate the JE incorporated image reconstruction method in MP activity estimation. The proposed technique is expected to contribute to the growing clinical applications of cardiac PET/MR imaging [8].

II. Materials and Methods

In this study, we simulated both the cardiac-gated MP PET imaging data with and without a perfusion defect and the corresponding MR images. For each given cardiac gate, we performed maximum a *posteriori* (MAP) reconstruction using the JE between the PET and MR images as the prior. To quantitatively evaluate the reconstructed MP images, polar maps were created for the left ventricle (LV) myocardial activities. The tradeoffs between noise versus bias on the polar map segments and the tradeoff between noise and lesion contrast recovery were used to compare the images reconstructed from the JE MAP method and the conventional maximum likelihood (ML) method.

A. PET Data Simulation

Using the 4D XCAT phantom [9], we simulated two cardiac gated MP imaging datasets, one with normal perfusion and the other with regionally reduced perfusion. The perfusion defect was a transmural defect spanning 40º over the anterior-lateral region and 1.5 cm over the long-axis direction. Its activity was 30% less than the normal activity. The time activity curves (TACs) of the blood pool, myocardium, and other organs were extracted from Rb-82 PET images of 5 patients with normal cardiac function [10]. They were smoothed and averaged to acquire a set of TACs representing the typical Rb-82 biodistribution. Analytical simulations were performed to simulate noise-free PET data of 8 cardiac gates. The noise-free sinograms were scaled to 5-min cumulated activity after pre-scan delay of ~30 sec to avoid high blood pool activity. For both normal and abnormal perfusion cases, Poisson noise realizations were implemented.

Manuscript received November 15, 2013. This work was supported in part by the U.S. National Science Foundation under grant ECCS-1228091.

J. Tang (e-mail: jtang@oakland.edu) and X. Wang are with the Department of Electrical and Computer Engineering, Oakland University, Rochester, MI 48309 USA.

N. A. Karakatsanis and A. Rahmim are with the Department of Radiology, The Johns Hopkins University, Baltimore, MD 21287 USA.

L. Lu is with the School of Biomedical Engineering, Southern Medical University, Guangzhou, Guangdong, China.

B. MR Image Simulation

The MRI simulation was performed using the open source MRI simulator SIMRI [11], based on the Bloch equation. We modified the simulator to take the T1, T2, and proton density maps created using the XCAT phantom, with known tissue values. SIMRI takes into account the main static field value and enables realistic simulations of the chemical shift artifact including off-resonance phenomena. To simulate a protocol used in the clinical PET/MRI, we specified the sequence to be 3D T1-weighted (turbo spin echo, echo time/repetition time = 2.3ms/4ms) with low flip angle of 2º. Eight cardiac gates were simulated to match the simulated PET data.

C. Joint Entropy Incorporated PET Image Reconstruction

We developed a closed-form PET image reconstruction algorithm incorporating the anato-functional JE prior within the one-step-late (OSL) MAP expectation-maximization (EM) approach [7]. For a given cardiac gate, we applied this Bayesian technique for MP image reconstruction, with the JE term $H(\mathbf{X},\mathbf{Y})$ from the PET image intensity $\mathbf{X}$ and MR image intensity $\mathbf{Y}$. The JE was calculated based on non-parametric, Parzen estimation of the probability density function, using superposition of Gaussian densities centered on samples across each image.

The image reconstruction process was to maximize the log-posterior probability: $\log P(\mathbf{g}\,|\,\mathbf{X}) - \beta H(\mathbf{X},\mathbf{Y})$, where $P(\,)$ indicates the probability of the variable enclosed in parenthesis, $\mathbf{g}$ is the measured data, and β is the weighting factor. Modeling Poisson statistics, and utilizing the OSL EM approach, we arrived at the closed-form MAP EM algorithm:

$$x_i^{\text{new}} = \frac{x_i^{\text{old}}}{\sum_j c_{ij} + \beta \frac{\partial H(\mathbf{X},\mathbf{Y})}{\partial x_i}\Big|_{x_i = x_i^{\text{old}}}} \sum_j \frac{c_{ij} g_j}{\sum_i c_{ij} x_i^{\text{old}}} , \qquad (1)$$

where g_j is the data in bin j, and c_{ij} represents an element of the system matrix modeling the contribution of voxel i to the projection bin j.

As we focused on cardiac area, the JE and its derivative as shown in Eqn. (1) was calculated on a cuboid covering the heart region. This saved calculation time and avoided possible involvement of other regions.

D. Evaluation Metrics

To quantitatively evaluate the performance of the JE MAP algorithm and compare it with the ML algorithm, we used the tradeoff between the noise and bias on the polar map (and its 5 segments) of the reconstructed normal MP images. For the whole polar map and its each segment, we calculated the normalized mean square error (NMSE) as a measure of bias:

$$\text{NMSE} = \left(\frac{\bar{X} - \bar{X}_{true}}{\bar{X}_{true}} \right)^2 , \qquad (2)$$

where $\bar{X} \triangleq \frac{1}{N}\sum_{i=1}^{N} X_i$, X_i denotes the i th reconstructed voxel activity value, N is the number of voxels in the region under consideration; and $\bar{X}_{\text{true}}$ denotes the reference true mean activity value. The normalized standard deviation (NSD) was calculated to measure noise

$$\text{NSD} = \frac{\sqrt{\frac{1}{N-1}\sum_{i=1}^{N}\left(X_i - \bar{X}\right)^2}}{\bar{X}} , \qquad (3)$$

where X_i and $\bar{X}$ were defined as those in Eqn. (2).

To evaluate the ability of defect classification, we calculated the contrast of between the lesion areas on the polar maps with and without the perfusion defect. The regional contrast was defined by

$$\text{Contrast} = \frac{\bar{X}_N - \bar{X}_D}{\bar{X}_N + \bar{X}_D} , \qquad (4)$$

where $\bar{X}_N$ and $\bar{X}_D$ are the average values on the lesion covered area of the polar maps with normal (N) and defect (D) MP, respectively. The contrast recovery ratio was calculated as the ratio between the contrast estimated from the reconstructed image and the true contrast.

III. Results

We present the results from the end-diastole gate, as those from other gates are similar. The simulated cardiac gated end-diastolic frame MR image and the corresponding noise-free reconstructed image with the perfusion defect are shown in Fig. 1. The perfusion defect has no anatomical correspondence in the MR image.

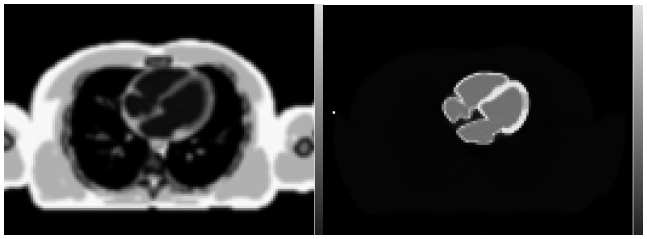

(a) (b)

Fig. 1. Transaxial slice of (a) the simulated cardiac-gated MR image, end-diastolic frame, and (b) the corresponding noise-free reconstructed PET image with the perfusion defect.

The short-axis view zoomed to the LV region of the reconstructed noise images (with the perfusion defect) from the ML and the JE MAP algorithms are shown in Fig. 2. The line profiles (crossing the center of the anterior-lateral defect region) demonstrate the reduced noise resulted by the JE MAP algorithm. In Fig. 3, we plot the polar maps of the images without and with the perfusion defect, reconstructed from the ML and the JE MAP algorithms, respectively. The line profiles crossing the center of the lesion region are shown to compare the polar maps.

In Fig. 4, we show the noise versus bias along with iteration number curves for the polar map and its segments. The JE MAP algorithm results in improved performance in terms of the tradeoff, compared to the ML algorithm. In Fig. 5, the noise versus contrast recovery ratio curves are plotted. The JE MAP algorithm results in much lower noise while achieving

contrast recovery ratio close to that from the ML algorithm at later iterations.

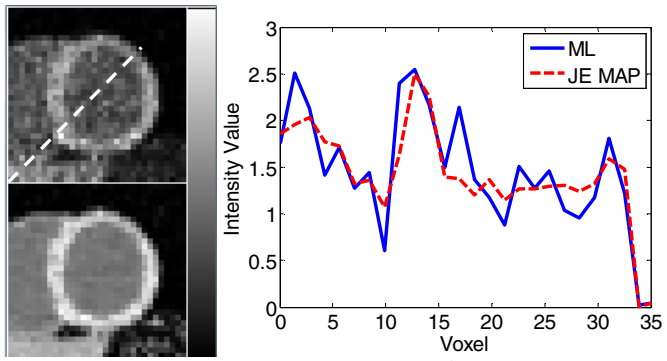

(a) (b)

Fig. 2. (a) Short-axis view of reconstructed images zoomed to the LV region (with the perfusion defect) from using the ML (top) and the JE MAP (bottom) algorithms; (b) The corresponding line profiles.

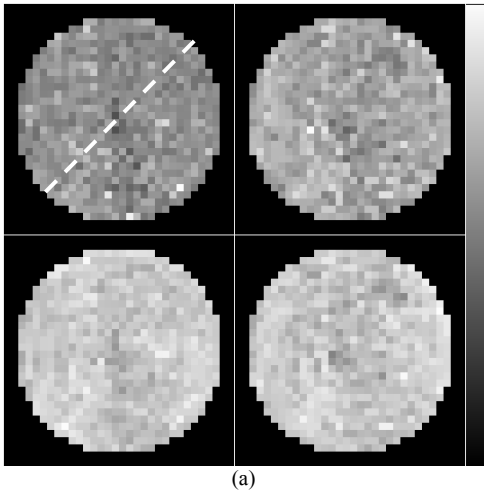

(a)

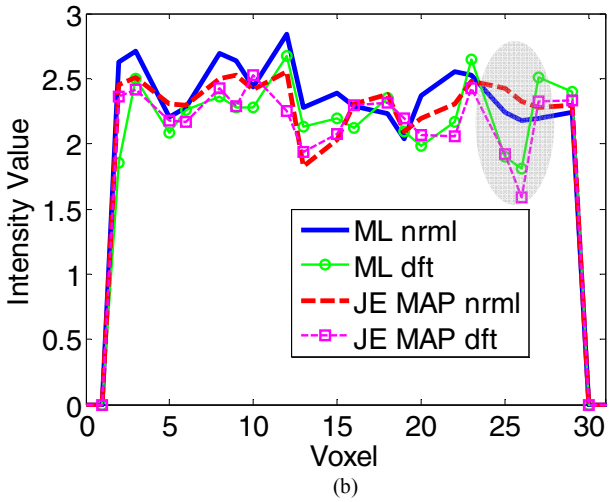

(b)

Figure 3: (a) LV polar maps made for images reconstructed from the ML algorithm (without and with perfusion defect, top left and top right) and the JE MAP algorithm (without and with perfusion defect, bottom left and bottom right); (b) The corresponding line profiles crossing the defect on the anterior-lateral region, defect area shaded.

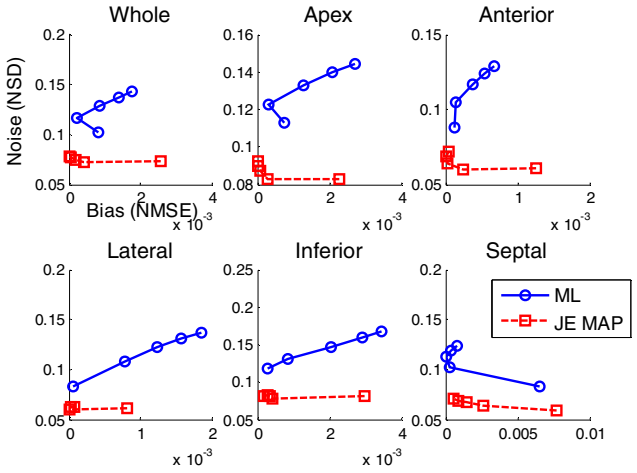

Fig. 4. Noise vs bias along with iteration number plots for the whole polar map and its 5 (apex, anterior, lateral, inferior, and septal) segments, from images reconstructed using the ML and the JE MAP algorithms.

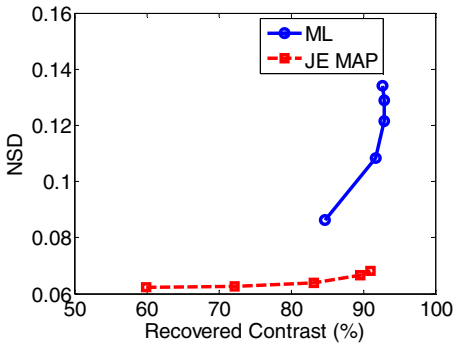

Fig. 5. Noise versus contrast recovery ratio along with iteration plots for the defect region on the polar map, from images reconstructed using the ML and the JE MAP algorithms.

IV. Conclusions

We applied the MAP algorithm which incorporates the anato-functional JE as the prior to gated MP PET image reconstruction. Using realistically simulated PET data and corresponding MR images we quantitatively demonstrated improved performance on estimating MP activity and recovering lesion contrast. The image reconstruction approach will have promising clinical applications especially in the emerging integrated cardiac PET/MR imaging.

Acknowledgment

We thank Eric Stevens for computational support.

References

[1] B. J. Pichler, A. Kolb, T. Nagele, and H. P. Schlemmer, "PET/MRI: paving the way for the next generation of clinical multimodality imaging applications," *J Nucl Med,* vol. 51, pp. 333-6, Mar 2010.

[2] G. Delso, A. Martinez-Moller, R. A. Bundschuh, S. G. Nekolla, and S. I. Ziegler, "The effect of limited MR field of view in MR/PET attenuation correction," *Med Phys,* vol. 37, pp. 2804-12, Jun 2010.

[3] V. Schulz, I. Torres-Espallardo, S. Renisch, Z. Hu, N. Ojha, P. Bornert, M. Perkuhn, T. Niendorf, W. M. Schafer, H. Brockmann, T. Krohn, A. Buhl, R. W. Gunther, F. M. Mottaghy, and G. A. Krombach, "Automatic, three-segment, MR-based attenuation correction for whole-

body PET/MR data," *Eur J Nucl Med Mol Imaging,* vol. 38, pp. 138-52, Jan 2011.

[4] C. Catana, T. Benner, A. van der Kouwe, L. Byars, M. Hamm, D. B. Chonde, C. J. Michel, G. El Fakhri, M. Schmand, and A. G. Sorensen, "MRI-assisted PET motion correction for neurologic studies in an integrated MR-PET scanner," *J Nucl Med,* vol. 52, pp. 154-61, Jan 2011.

[5] B. Guerin, S. Cho, S. Y. Chun, X. Zhu, N. M. Alpert, G. El Fakhri, T. Reese, and C. Catana, "Nonrigid PET motion compensation in the lower abdomen using simultaneous tagged-MRI and PET imaging," *Med Phys,* vol. 38, pp. 3025-3038, Jun 2011.

[6] B. Bai, Q. Li, and R. M. Leahy, "Magnetic resonance-guided positron emission tomography image reconstruction," *Semin Nucl Med,* vol. 43, pp. 30-44, Jan 2013.

[7] J. Tang and A. Rahmim, "Bayesian PET image reconstruction incorporating anato-functional joint entropy," *Phys Med Biol,* vol. 54, pp. 7063-75, Dec 2009.

[8] S. G. Nekolla, A. Martinez-Moeller, and A. Saraste, "PET and MRI in cardiac imaging: from validation studies to integrated applications," *Eur J Nucl Med Mol Imaging,* vol. 36 Suppl 1, pp. S121-30, Mar 2009.

[9] W. P. Segars, D. S. Lalush, and B. M. W. Tsui, "A realistic spline-based dynamic heart phantom," *IEEE Trans Nucl Sci,* vol. 46, pp. 503-506, Jun 1999.

[10] J. Tang, A. Rahmim, R. Lautamaki, M. A. Lodge, F. M. Bengel, and B. M. Tsui, "Optimization of Rb-82 PET acquisition and reconstruction protocols for myocardial perfusion defect detection," *Phys Med Biol,* vol. 54, pp. 3161-71, May 2009.

[11] H. Benoit-Cattin, G. Collewet, B. Belaroussi, H. Saint-Jalmes, and C. Odet, "The SIMRI project: a versatile and interactive MRI simulator," *J Magn Reson,* vol. 173, pp. 97-115, Mar 2005.